Electronic Supplementary Material (ESI) for Chemical Communications.

Supporting Information

Hollow carbon anchored highly dispersed Pd species for selective hydrogenation of 3-nitrostyrene: metal-carbon interaction

Yang Lou, Jia Xu, Honglu Wu, Jingyue Liu*

Department of Physics, Arizona State University, Tempe, Arizona 85287, United States

Corresponding author

Email: jingyue.liu@asu.edu

Contents:

1. Catalyst preparation and characterization

1. 1 Preparation of single atom catalysts

Pd clusters/single atoms were dispersed onto, via an adsorption method[1-3], the surfaces of commercial carbon black (XC-72) and hollow nanocarbons (h-NCs). In details:

1) Preparation of h-NCs: h-NCs were synthesized via catalytic reforming/decomposition of ethanol on the surfaces of the ZnO nanowires. The details of synthesizing ZnO nanowires are discussed in the Ref.[4] In this work, we used the ZnO nanowires as templates to synthesize mesoporous h-NCs. The pre-formed ZnO nanowires were loaded into a high temperature furnace tube, which was then heated to 500 ^{o}C. A mixture of nitrogen, water and ethanol was then introduced into the furnace tube. Ethanol reforming as well as decomposition occurs on the surfaces of the ZnO nanowires. Such catalytic reactions result in residues of carbonaceous species uniformly coating the ZnO nanowires. Because of this coking induced deactivation, the thickness of the deposited carbonaceous layers is self-limiting. By controlling the reaction time, one can control the thickness of the deposited carbonaceous layers. After the desired thickness of the carbonaceous layers was obtained the ZnO (nanowires) were evaporated at a temperature of 750 ^{o}C for 6 h with a flowing gas mixture of H_2/Ar to produce the hollow carbon tubes with mesopores on the sidewalls.

2) Pd/h-NC preparation: The h-NCs were firstly dispersed in the ethanol and then the corresponding Pd precursors (Palladium (II) chloride, Sigma-Aldrich) were slowly dropped into the ethanol (Sigma-Aldrich). After stirring at room temperature for 2 hours, the ethanol was slowly evaporated out and then the obtained catalyst was dried at 60 ^{o}C for 12 hours in air without further calcination in case the structure of h-NC was collapsed at high temperature. The actual Pd loading is 0.48 wt.% measured by ICP-MS.

3) Pd/XC-72: The carbon black (XC-72) was firstly dispersed in the ethanol and then the corresponding Pd precursors (Palladium (II) chloride, Sigma-Aldrich) were slowly dropped into the ethanol (Sigma-Aldrich). After stirring at room temperature for 2 hours, the ethanol was slowly evaporated out and then the obtained catalyst was dried at 60 ^{o}C for 12 hours in air. The actual Pd loading is 0.59 wt.% measured by ICP-MS.

4) Pd_1/h-NC SAC preparation: The h-NCs will be well dispersed in ethanol first since the h-NCs are hydrophobic. 100 ml DI water are added into above mixture solution of ethanol and h-NCs and then the ethanol (Sigma-Aldrich) will be evaporated out at 80 ^{o}C. After these steps, the originally hydrophobic h-NCs can be turned to be hydrophilic. The pH value of the solution of h-NCs will be precisely controlled in the range of 3.0 to 3.5 by adding the acid solutions. The precursors of Pd (Palladium (II) chloride, Sigma-Aldrich) will be pumped into the solution at the speed of around 0.5 ml/min and then the above solution containing Pd and h-NCs will be aged for 2 hours at room temperature. After washing the samples for at least three times in order to eliminate the residual Cl^- ions, the obtained powders will be dried at 60 ^{o}C for 12 h in air. The actual Pd loading was 0.19 wt.% by ICP-MS.

1. 2 Evaluation of the catalytic performance

The hydrogenation of 3-nitrostyrene was conducted in a Parr high-pressure reactor (Parr 4560 reactor-100 ml). Before the activity test, the catalyst was first introduced into the reactor, to which 8 ml ethanol was added, and then the reactor was charged with 5 bar hydrogen and heated at 40 °C for 40 min to allow for the reduction treatment of the catalyst. After the catalyst was activated and the reactor was cooled to room temperature, the 3-nitrostyrene substrate, internal standard O-xylene and 8 ml ethanol were fed into the

reactor. Then, the reactor was flushed with 5 bar hydrogen for 11 times to purge air. After being sealed, the autoclave was charged with H_2 until 5 bar, then was heated to 40 °C under stirring to initiate the reaction. The molecular ratio of Pd atoms to 3-nitrostyrene molecules is 0.14%. After the desired reaction time was reached, the liquid products were cooled to room temperature and then collected by using filter paper and analyzed by a gas chromatography (Agilent GC 7890A with HP-5 column) equipped with an auto sampler (Agilent G4513A). The peaks were calibrated by the standard chemicals from Sigma-Aldrich. The TOF value was separately measured by keeping the substrate conversion below 25% by tuning the molecular ratio of Pd atoms to 3-nitrostyrene molecules and the calculation of the TOF was based on the total Pd loading in the catalyst.

1. 3 Kinetic measurements

The reaction rates (calculated based on equation (1)) of the synthesized catalysts were measured under a reaction condition of 9.0 vol.% H_2, 4.5 vol.% O_2, and He balance with an weight hourly space velocity of 19, 140 l/g•h at 20 ºC and 50 ºC. In order to eliminate the thermal and diffusion effects, the catalysts were diluted with inert SiO_2 and the conversion rate is controlled to below 15%.

$$r = \frac{C_{H_2} \cdot X_{H_2} \cdot V \cdot P_{atm}}{m_{cat} \cdot R \cdot T} (mol \cdot s^{-1} \cdot g_{cat}^{-1}) \qquad (1)$$

Where r is the reaction rate of catalysts and supports; m_{cat}: mass of catalyst in the reactor bed (g); C_{H2}: concentration of H_2 in the feed gas; V: total flow rate (m^3/s); X_{H2}: conversion rate of H_2; R: molar gas constant (8.314 Pa • m^3 • mol^{-1} • K^{-1}); T: temperature (K); P_{atm}: atmospheric pressure (101.3 KPa); N_A: Avogadro constant (6.02×10^{23} mol^{-1}).

1. 4 Catalyst Characterization

The loading level of the Pd was measured by a ThermoFinnegan iCAP Q quadrupole ICP-MS with CCT (Collision Cell Technology). Samples were run in KED (Kinetic Energy Discrimination) mode, with in-line aspiration of a multi-element internal standard.

Sub-angstrom resolution high-angle annular dark-field (HAADF) scanning transmission electron microscopy (STEM) images were obtained on a JEM-ARM200F TEM/STEM with a guaranteed resolution of 0.08 nm. Before microscopy examination, the catalyst powders were ultrasonically dispersed in ethanol and then a drop of the solution was put onto a copper grid coated with a thin lacey carbon film.

The X-ray photoelectron spectroscopy (XPS) investigation was conducted on a Vacuum Generators 220i-XL using a mono-chromated Al Kα X-ray source (1486.6 eV). The samples were mounted onto the double-sided adhesive tape on the sample holder. The XPS spectra of the selected elements were measured with the constant analyzer pass energy of 20.0 eV. All binding energies (BEs) were referred to the C 1s peak (284.6 eV). The deconvolution of the spectra was similar to our previous work.[5, 6]

Raman experiments were conducted on LabRam HR 800 using 532 nm laser. The deconvolution of the spectra was similar to ref.[7]

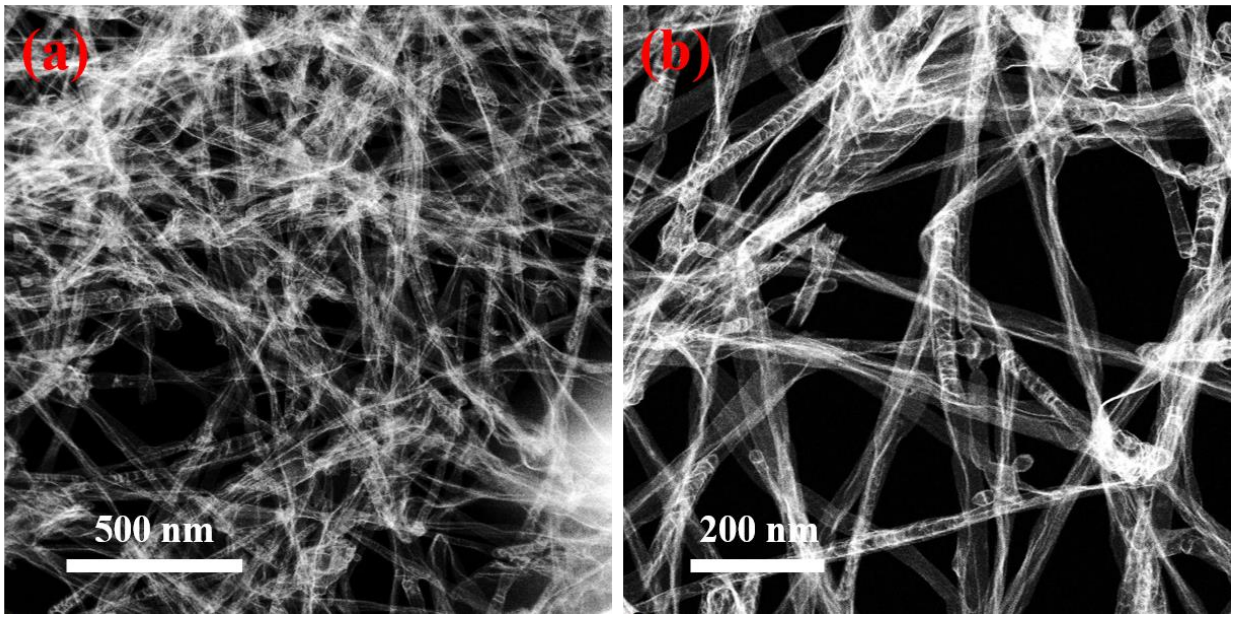

Figure S1 Aberration-corrected HADDF-STEM image (a-b) of h-NCs.

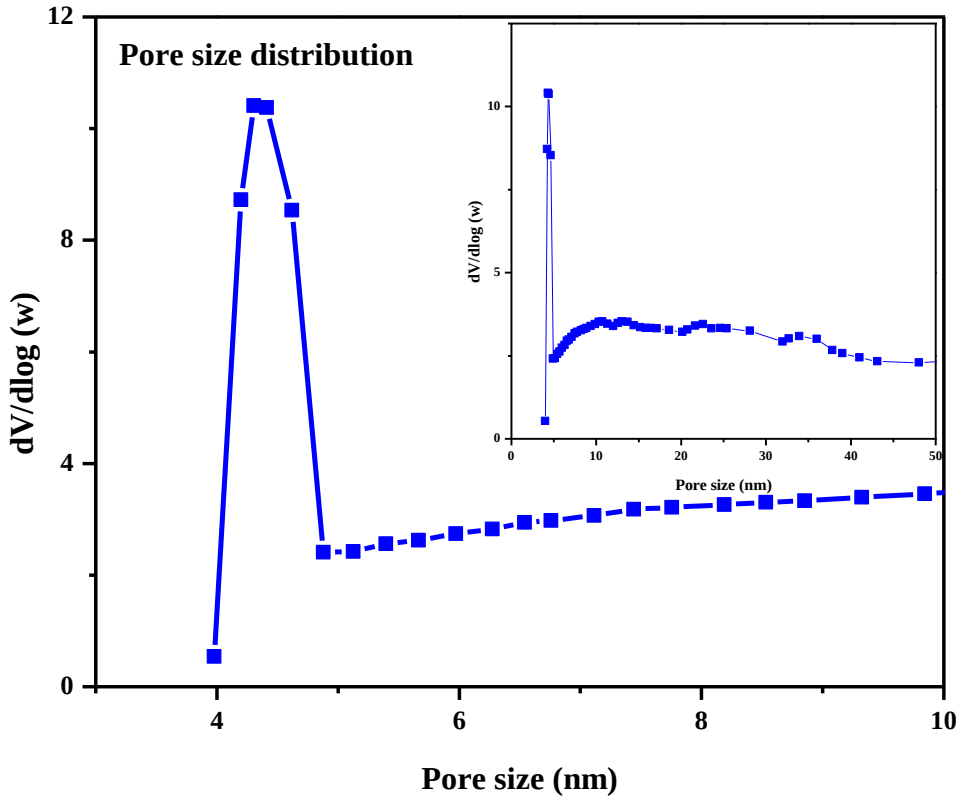

Figure S2 The pore size distribution of hollow nanocarbon. The average size of pores on the wall of the h-NCs is 4.3 nm.

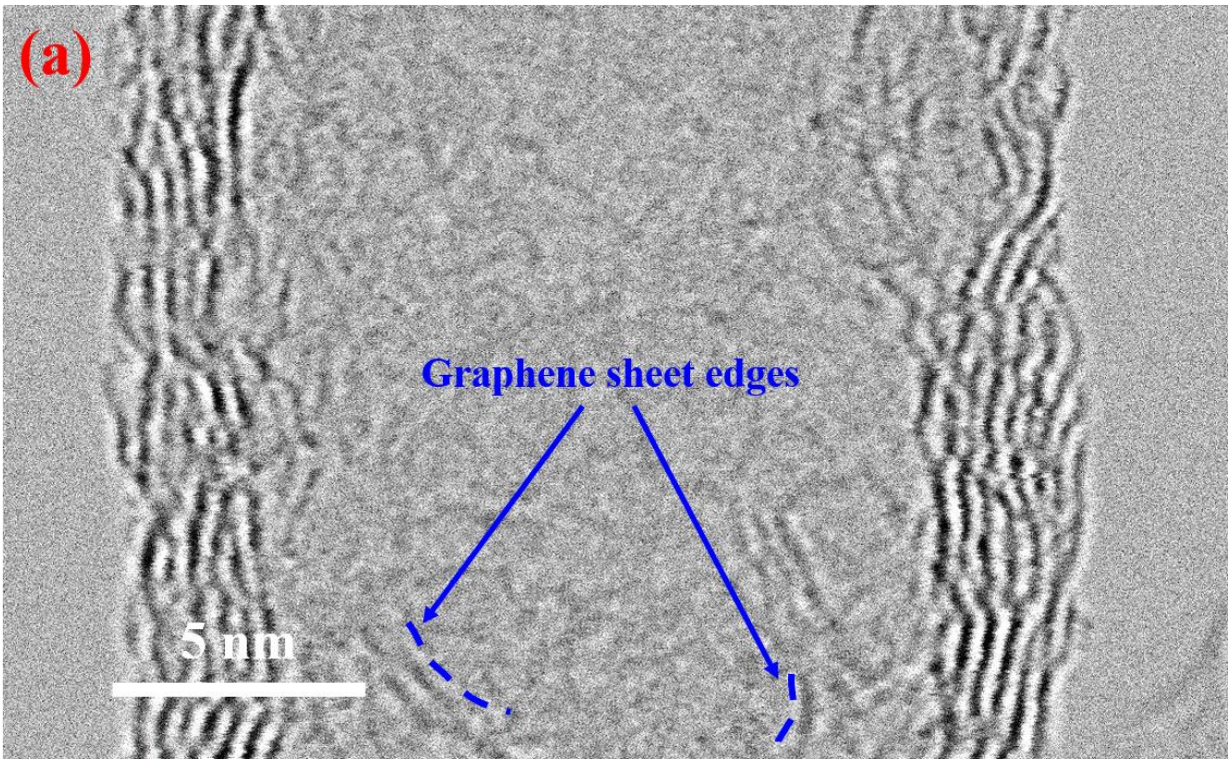
(a)
Graphene sheet edges
5 nm

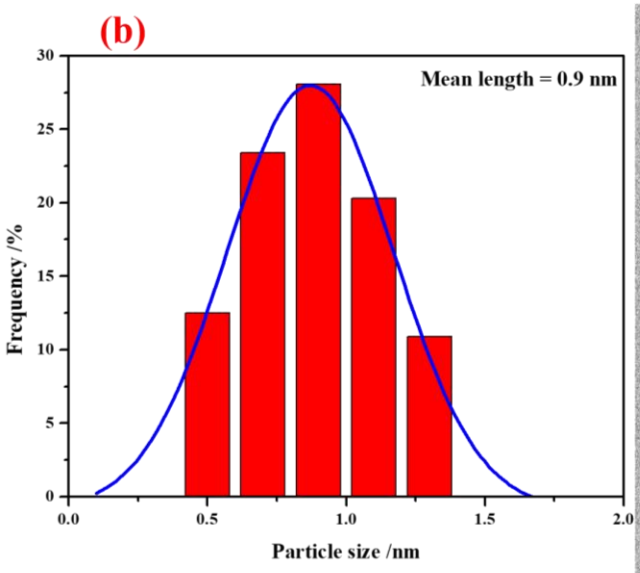
(b)
Mean length = 0.9 nm
Frequency /%
Particle size /nm
0
5
10
15
20
25
30
0.0
0.5
1.0
1.5
2.0

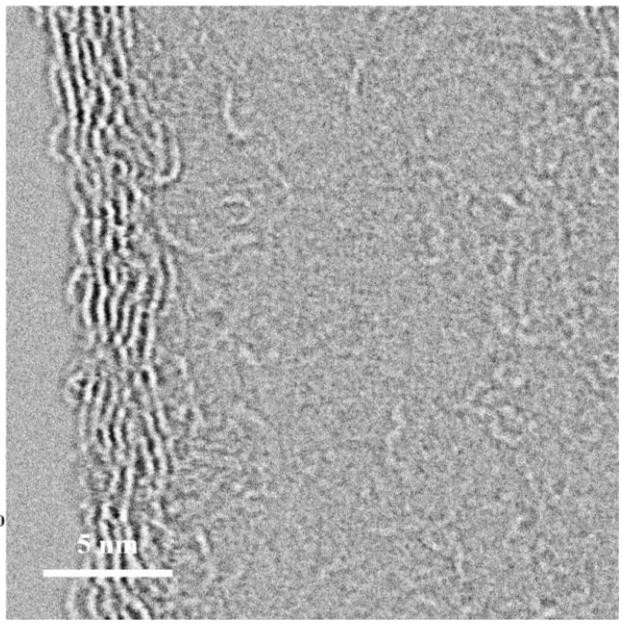
5 nm

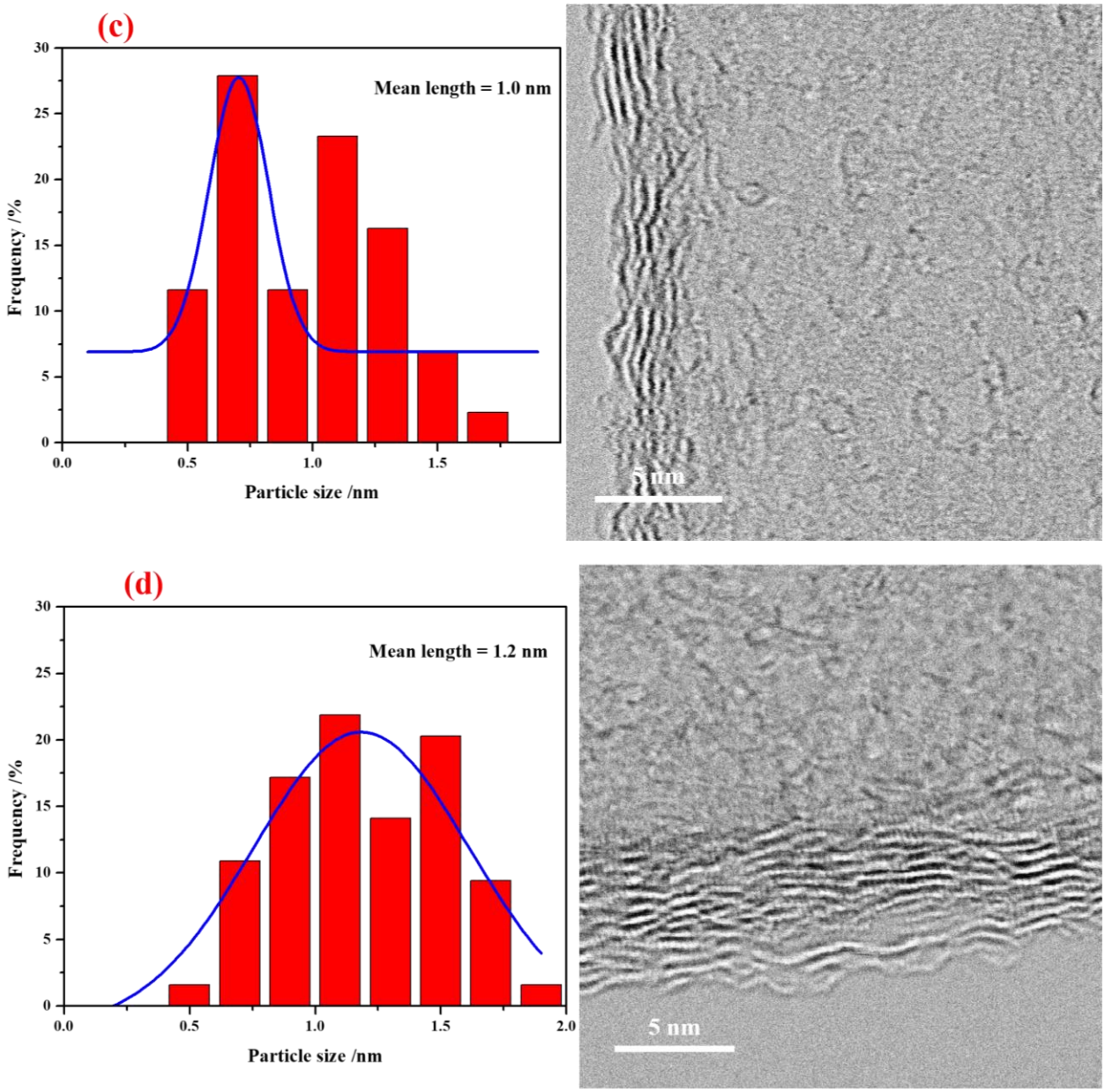

Figure S3 The Aberration-corrected STEM images of hollow nanocarbon: defects on the h-NCs (a), the defects on the edge of graphene sheets (b) and the length of graphene sheets (c-e).

The synthesized h-NCs is composed of the hypercross-linked graphene sheets, which create the highly disordered structure, high surface area and tube-type morphology (more images shown below). The hypercross-linked graphene sheets exhibit high-density defects including the point defects, defect line, multi-vacancies and so on as shown in the Figure S3 (a). The graphene sheets are in the range of 0.5 to 3.1 nm with the average length of 1.0 ± 0.2 nm as show in the (b-d).

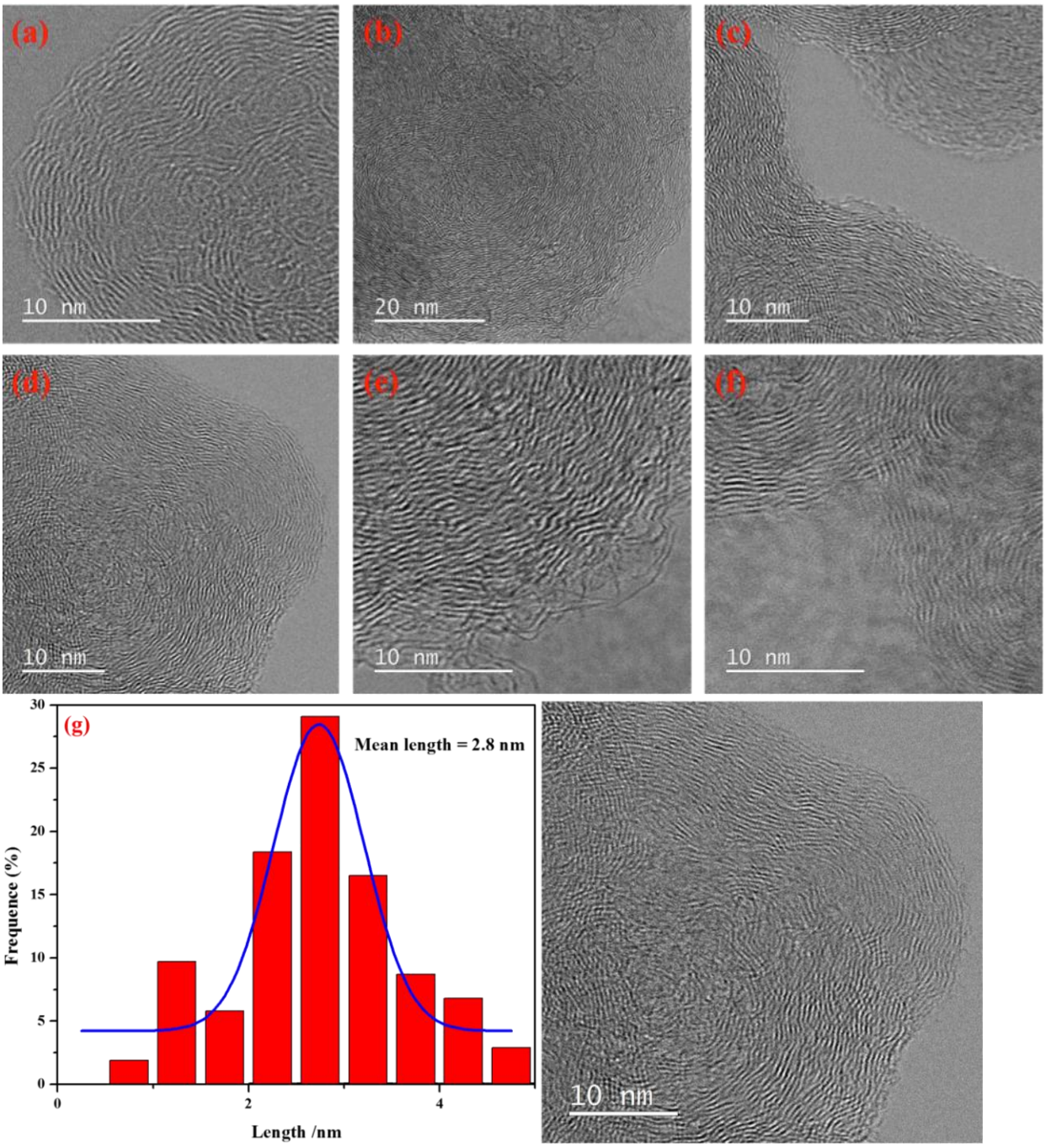
(a)
10 nm
(b)
20 nm
(c)
10 nm
(d)
10 nm
(e)
10 nm
(f)
10 nm
(g)
Mean length = 2.8 nm
Frequence (%)
Length /nm
0
5
10
15
20
25
30
0
2
4
10 nm

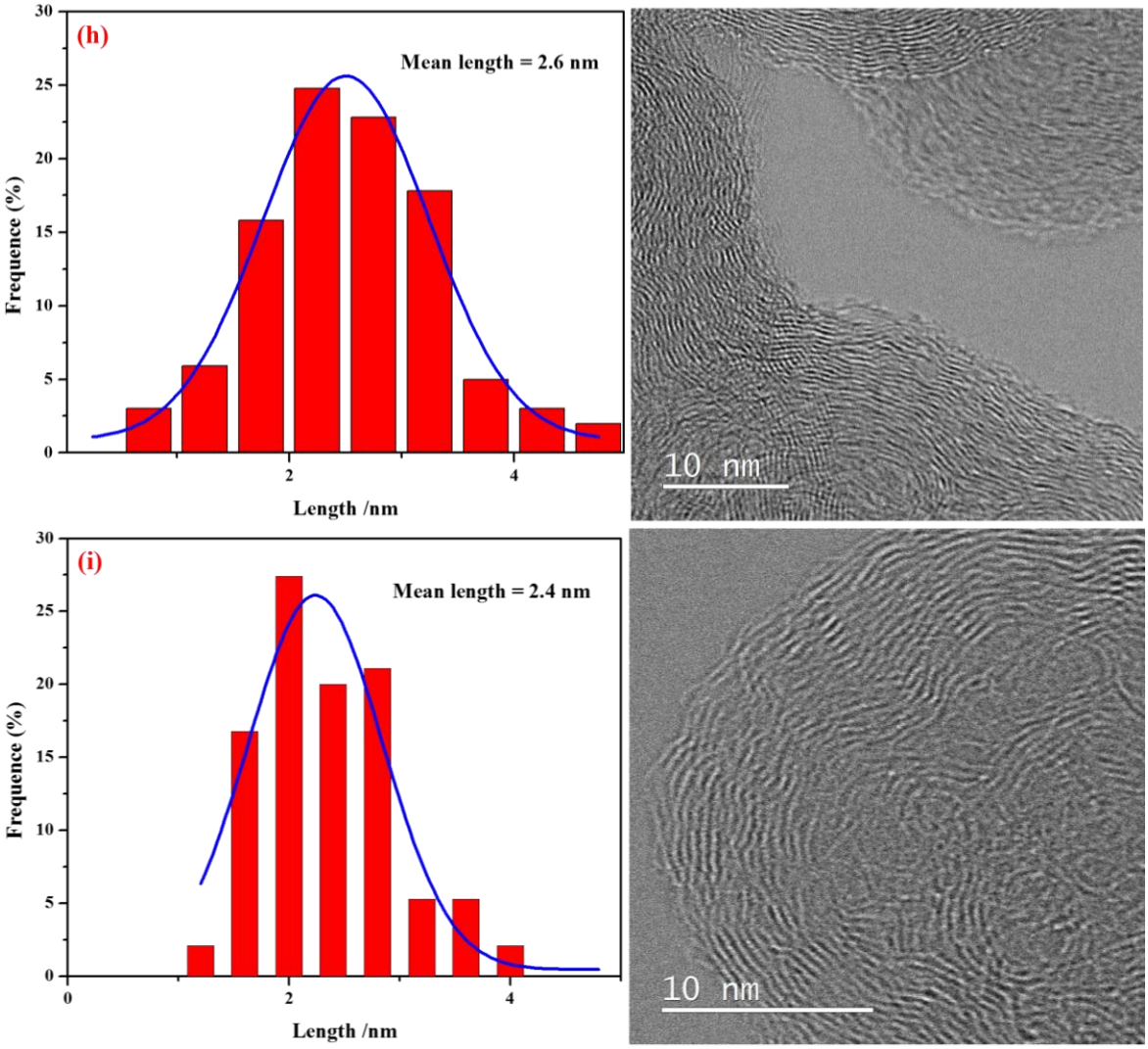

Figure S4 The high-angle annular bright-field scanning transmission electron microscope (HAABF-STEM) images of XC-72 (a-f), and the length of graphene sheets (g-i).

As clearly shown in Figure S4 (a-f), the XC-72 is composed of aggregated spherical particles with onion-like graphitized structures. The graphene sheets are in the range of 0.8 to 5.0 nm with the average length of 2.6 ± 0.2 nm as show in the (g-i). The data of statistical length is acquired by using the software to count the number and measure the length of graphene sheets.

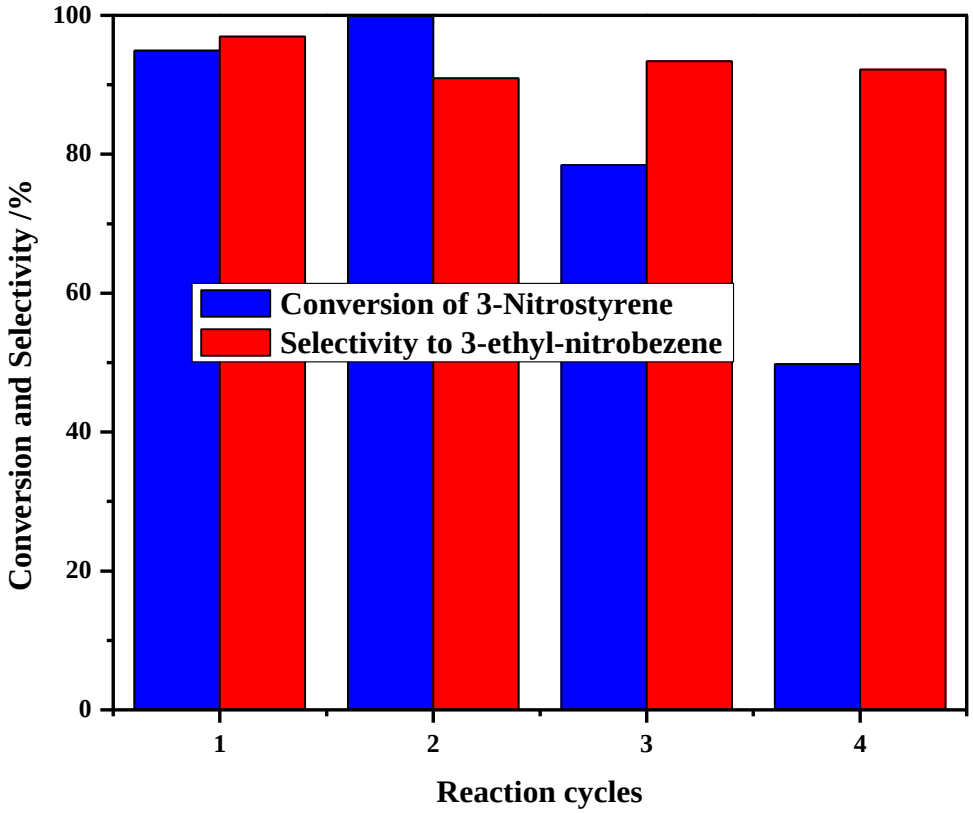

Figure S5 Recycling of the Pd/h-NC for the 3-nitrostyrene hydrogenation.

Reaction conditions: 40 °C/10min, 5 bar H_2, Pd/3-nitrostyrene ratio = 0.14%, catalyst weight = 5 mg.

There is no obvious change on the Pd particle size of used Pd/h-NC as in FigureS6, which indicates that the sintering of Pd particles should not be the reason for the loss of catalyst activity. Also, the leaching of Pd after reaction is negligible and not detectable. But there were obvious catalysts sticking on the filter paper for each cycle and the total catalysts we used for testing were only 5 mg since the h-NCs are very precious and very difficult to prepare in larger scale. Due to the amount of catalysts we used for testing is very low, the catalysts sticking on the filter paper may cause the obvious decrease on the total activity. Hence, the decrease on the conversion rate should be mainly from the loss of catalysts sticking on the surface of filter paper.

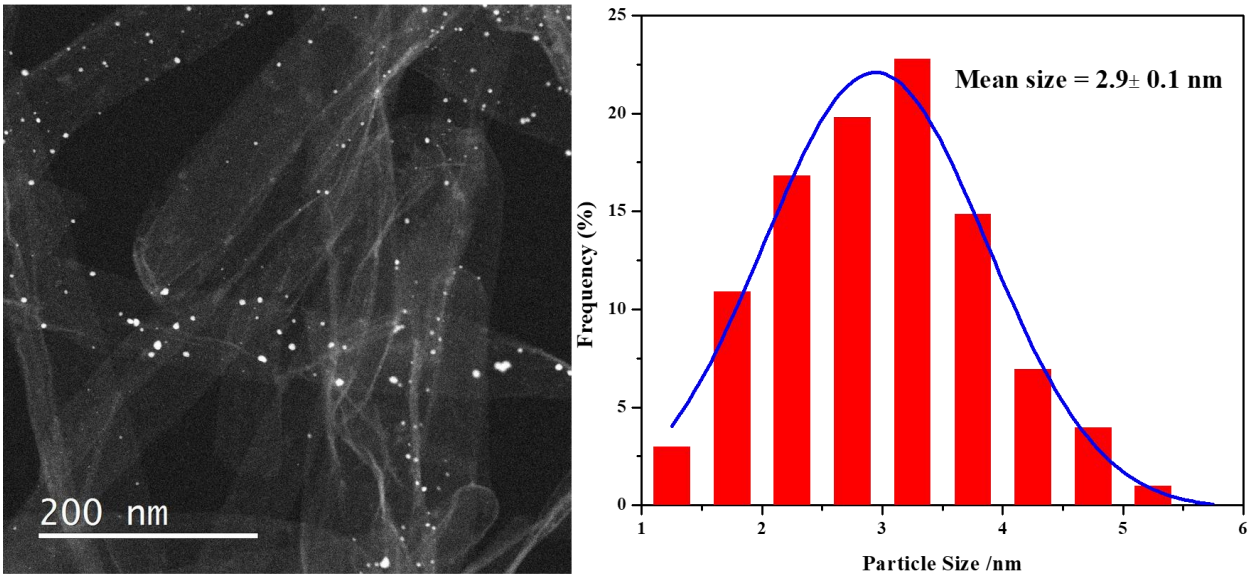

Figure S6 HAADF-STEM images and particle size distributions of used Pd/h-NC. The average particle size of Pd particles is 2.9 ± 0.1 nm while the average size of fresh catalyst is 2.8 ± 0.2 nm, which indicates that there was no obvious sintering during the catalytic reaction.

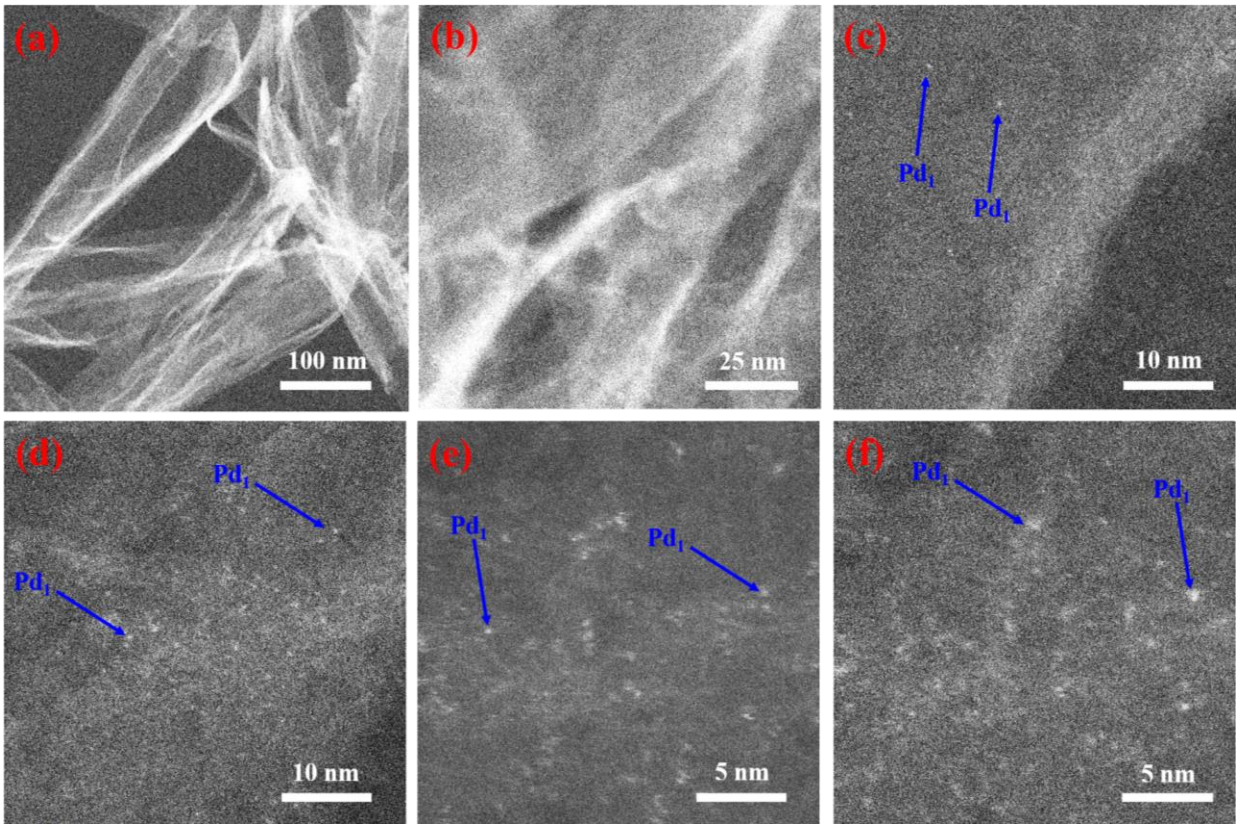

Figure S7 Aberration-corrected HAADF/STEM images of fresh Pd_1/h-NC SAC： Low magnification (a-b) and high magnification (c-f).

As clearly shown in Figure S7 (a-b), low-magnification HAADF-STEM images confirm the absence of any Pd particles or clusters in the fresh Pd_1/h-NC SAC (with Pd loading of 0.18 wt.%). The high-magnification HAADF-STEM images (b-f) confirm that the Pd atoms are atomically dispersed on the surfaces of the h-NCs support. By examining numerous low/high magnification HAADF-STEM images (a-f) obtained from different regions, we unambiguously conclude that the Pd_1/HC contains only isolated Pd atoms without any Pd particles or clusters dispersed onto the h-NCs supports.

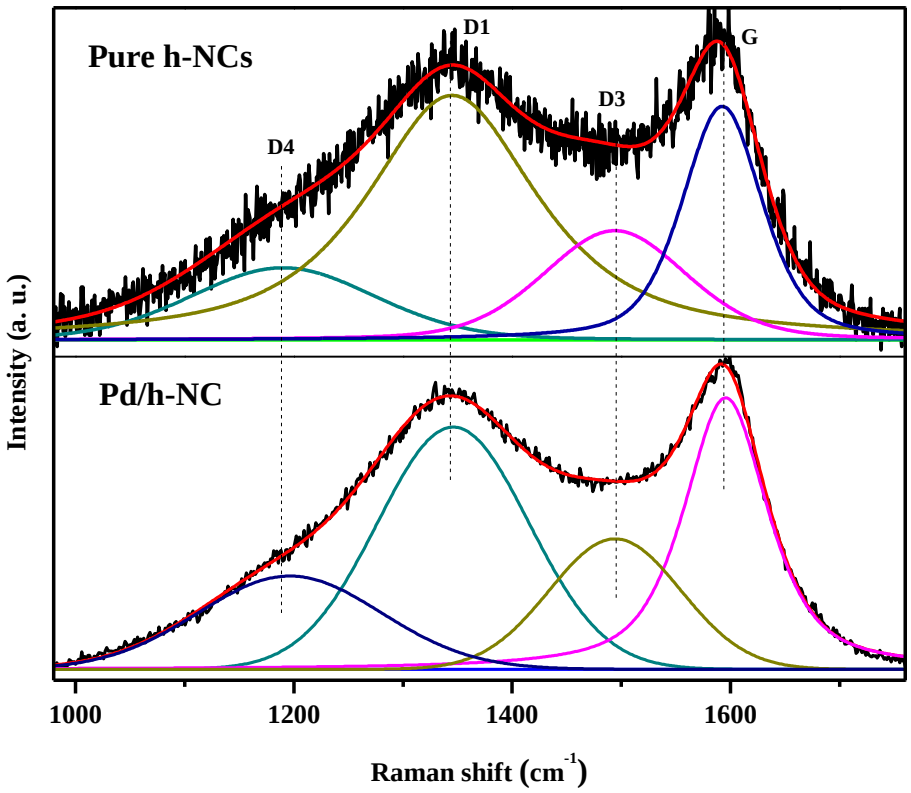

Figure S8 Raman spectra of pure hollow nanocarbon and Pd/h-NC.

The peaks at 1190 cm^{-1}, 1345 cm^{-1}, and 1508 cm^{-1} can be assigned to the D4, D1 and D3 band and the peak at 1591 cm^{-1} can be assigned to the G band.[8, 9] The D_1-band is associated with the defects within the carbon atom plane and the G-band is original from the sp^2-bonded carbon atoms.[10] The presence of D3 can be attributed to the stacking faults, changes in the interlayer spacing and the mixed breathing and asymmetric stretching vibrational modes of sp^2-carbons near defects causing out of the plane deformation.[11, 12] The broad component of D4 can be assigned to the amorphous impurities in the graphite materials.[13] The ratio between D1 and G band intensities (I_{D1}/I_G) can be used as an indication of the degree of disorder and the sp^3-hybridized carbon atoms within the structure. The pure carbon nanotubes used as the substrates to support Pd clusters exhibit a high I_{D1}/I_G ratio (1.1), which confirms that there are high-density defects in the structure of h-NCs.[7, 10, 14]

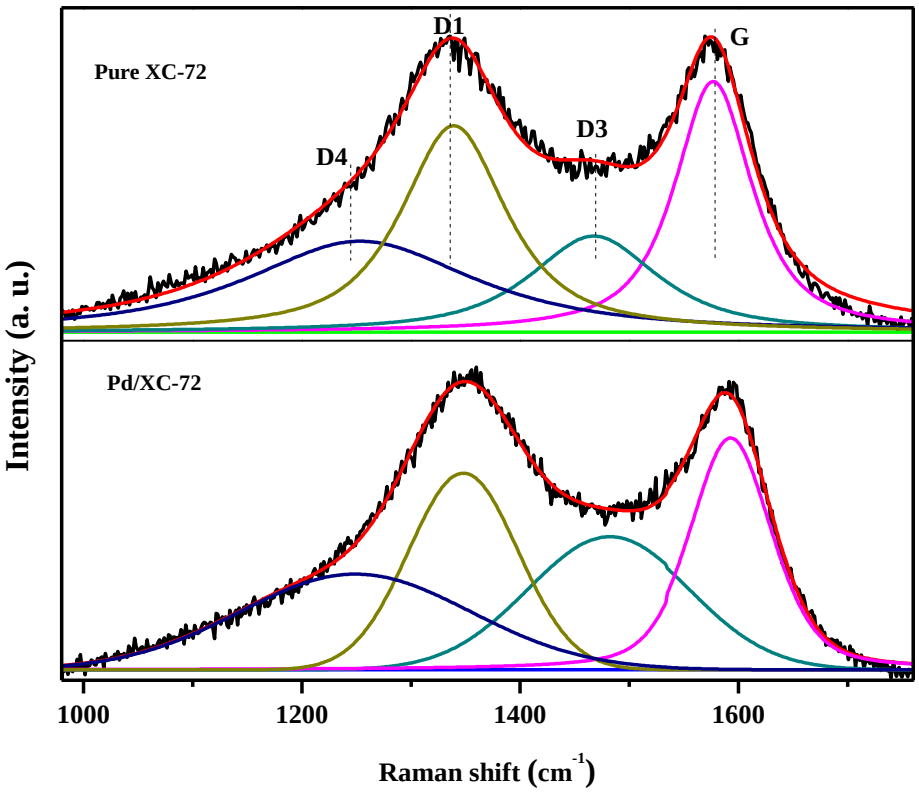

Figure S9 Raman spectra of pure XC-72 and Pd/XC-72.

The ratio between D1 and G band intensities (I_{D1}/I_G) of pure XC-72 is 0.85, which is in line with the previously reported data (0.84).[15] The ratio between D1 and G band intensities (I_{D1}/I_G) of Pd/XC-72 is decreased by 1%.

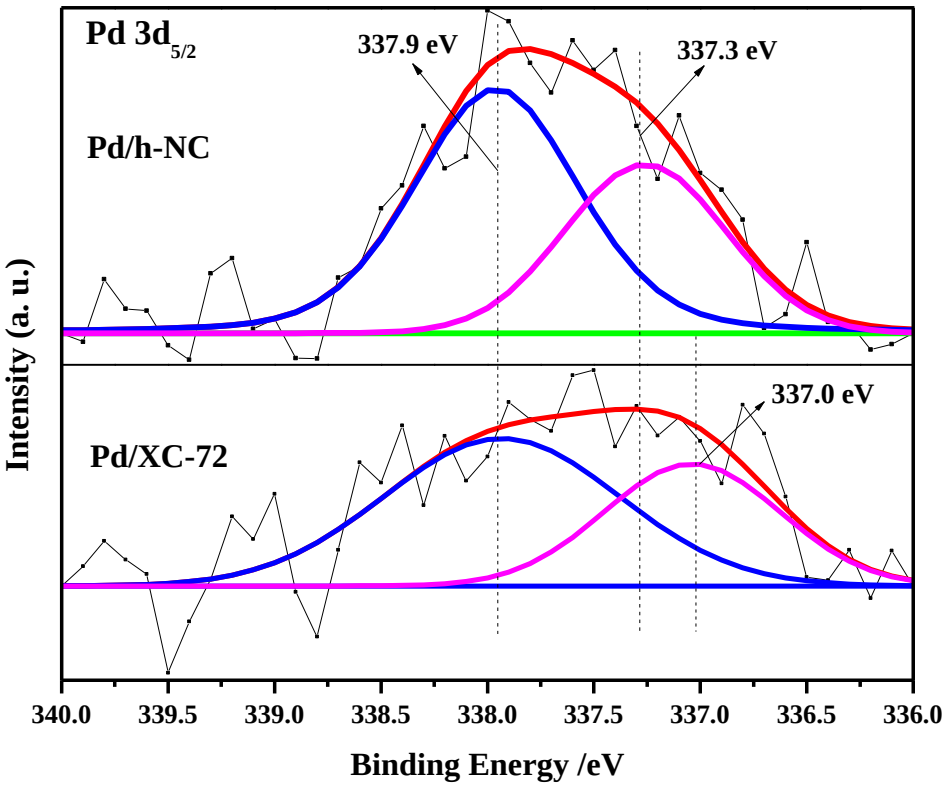

Figure S10 XPS Pd 3d spectra of: Pd/h-NC and Pd/XC-72.

As clearly shown in Figure S10, after the deconvolution of Pd $3d_{5/2}$ peak, there are two peaks located at 337.9 eV and 337.3 eV on the sample of 1.0 wt.% Pd/XC-72, which can be assigned to the oxidation states of PdO_2 and PdO, respectively.[16-21] These results indicate that the Pd species on the surface of XC-72 are mainly in the form of oxides and the formation of Pd oxides may mainly originate from the self-oxidation.[22] For the sample of 1.0 wt.% Pd/h-NC, there are two peaks located at 337.9 eV and 337.0 eV. The peak located at 337.9 eV can be assigned to the PdO_2 species. But the binding energy of peak at 337.0 eV is between the values reported in the literature for Pd^{1+} (335.5 eV) and Pd^{2+} (337.3 eV).[23] Therefore, this peak can be attributed to the electron-depleted Pd atoms (Pd^{n+}, $1< n <2$), resulting from the charge transfer from the Pd species to the carbon support.[24] The similar results have been also reported in the previous literature.[25]

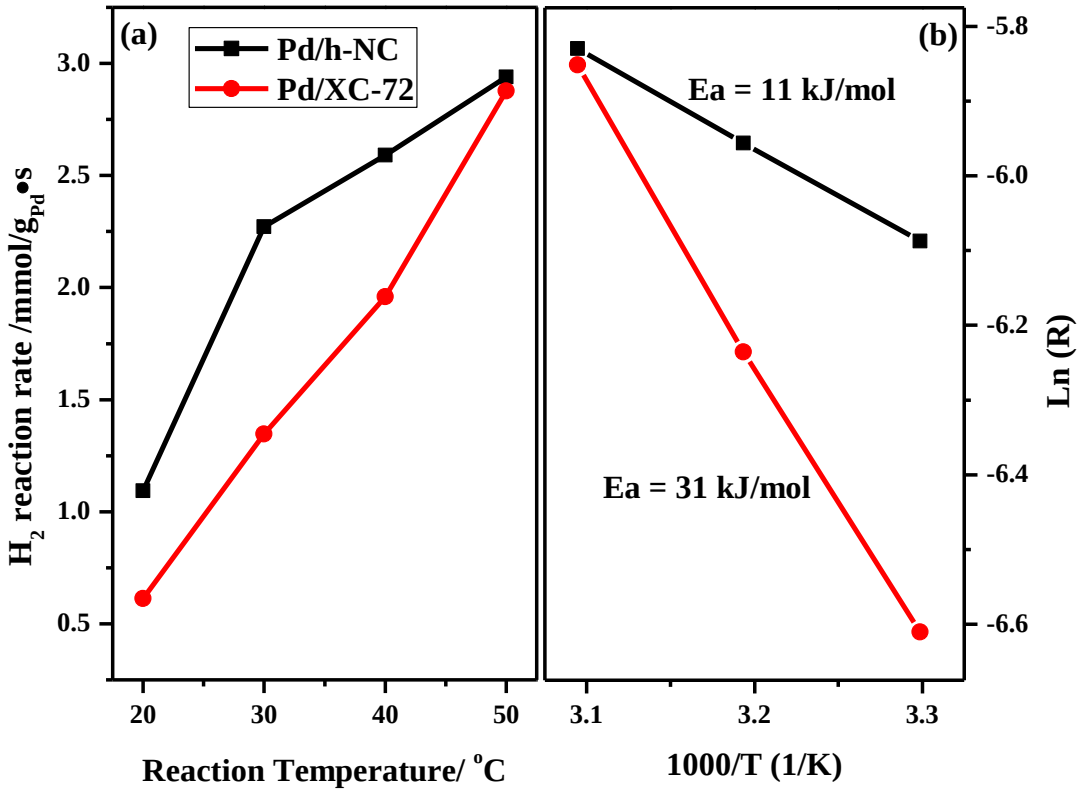

Figure S11 Specific rate of H_2 oxidation over Pd/h-NC and Pd/XC-72 (a); Apparent activation energy (Ea) of Pd/h-NC and Pd/XC-72 for H_2 oxidation (b). Feed gas composition: 9.0 vol % H_2, 4.5 vol % O_2, and He balance with a WHSV of 19, 140 L/g·h.

Table S1 Chemoselective hydrogenation of 3-nitrostyrene on Pd/h-NC compared with the most selective catalysts in the literature.

Catalyst	T/°C	H_2 pressure /bar	Solvent	3-EN Selectivity/%	3-NS TOF (1/h)	Reference
0.5Pd/COF	90	30.00	Heptane	100	76.6	Ref [26]
0.9Pd/CMP-1-H_2	50	3.00	Toluene	99	99	Ref [27]
$Pd_{13}Ga_5$	70	MC[1]	Methanol	99	0.03	Ref [28]
PdZn	70	MC[1]	Methanol	99	0.01	Ref [28]
Rh/HAP	25	1	1, 4-Dioxane	100	/	Ref [29]
Pt-Q@IL	25	1	THF	83	260	Ref [30]
Pd/h-NC	40	5	Ethanol	97	21,845	This work

1: 4-methyl-1-cyclohexene (MC) is used as the hydrogenation resource.

Table S2 Summary of the defect density and crystallite size of synthesized nano-Pd catalysts

Sample	La /nm[a]	Defect density[b]	Defect density[c]
h-NCs	6.6 (1.2[d])	2.27E+12 (6.94E+13[e])	7.21E+11 (2.21E+13[e])
1.0 wt.% Pd/h-NC	15.6	4.10E+11	1.31E+11
XC-72	14.2 (2.6[d])	4.96E+11 (1.48E+13[e])	1.58E+11 (4.71E+12[e])
1.0 wt.% Pd/XC-72	14.8	4.54E+11	1.45E+10

a: The crystallite size (La) is estimated based on the La (nm)=560*(El^4)*$(I_D/I_G)^{-1}$, El is the laser excitation energy used in the Raman experiment in eV units.[31] And the estimated value is normally larger than that of actual one.[32]

b: The defect density (n_a/cm^{-2}) is calculated by the formula of $n_a=(1/La)^2$.[31]

c: The defect density (n_a/cm^{-2}) is calculated by the formula of $n_a=10^{14}/\pi La^2$.[33, 34]

d: The crystallite size is calculated based on the STEM images as shown in Figure S3 and Figure S4.

e: The defect density is calculated based on crystallite size in the parenthese.

Based on two empirical formula models[31, 33, 34], it is very clear that the defect density of h-NCs is around 5 times higher than that of XC-72. After the deposition of Pd particles, the defect density of Pd samples is correspondingly decreased. Although the amount of defect density calculated based on the empirical formula model may not be exactly same as the actual defect density, but the trend is very clear that the h-NCs behave much higher density defects than that of XC-72, which is in line with our STEM images and raw Raman data.

Reference

(1) B. Qiao, J. Liu, Y. G. Wang, Q. Lin, X. Liu, A. Wang, J. Li, T. Zhang and J. Liu, *ACS Catal.* 2015, **5**, 6249-6254.
(2) Y. Lou and J. Liu, *Chem. Commun.* 2017, **53**, 9020-9023.
(3) Y. Lou and J. Liu, *Ind. Eng. Chem. Res.* 2017, **56**, 6916-6925.
(4) J. Xu and J. Liu, *Chem. Mater. 2016*, **28,** 8141-8148.
(5) Y. Lou, J. Ma, X. Cao, L. Wang, Q. Dai, Z. Zhao, Y. Cai, W. Zhan, Y. Guo, P. Hu, G. Lu and Y. Guo, *ACS Catal.* 2014, **4,** 4143-4152.
(6) Y. Lou, X. M. Cao, J. Lan, L. Wang, Q. Dai, Y. Guo, J. Ma, Z. Zhao, Y. Guo, P. Hu and G. Lu, *Chem. Commun.* 2014, **50,** 6835-6838.
(7) G. Wen, B. Wang, C. Wang, J. Wang, Z. Tian, R. Schlogl and D. S. Su, *Angew. Chem. Int. Ed.* 2017, **56,** 600-604.
(8) K. Gopinadhan, Y. J. Shin, I. Yudhistira, J. Niu and H. Yang, *Phys. Rev. B.* 2013, **88**, 195429.
(9) S. A. Chernyak, A. S. Ivanov, K. I. Maslakov, A. V. Egorov, Z. Shen, S. S. Savilov and V. V. Lunin, *Phys. Chem. Chem. Phys.* 2017, **19,** 2276-2285.
(10) L. Wang, Z. Sofer, D. Bousa, D. Sedmidubsky, S. Huber, S. Matejkova, A. Michalcova and M. Pumera, *Angew. Chem. Int. Ed.* 2016, **55,** 13965-13969.
(11) S. Maldonado, S. Morin and K. J. Stevenson, *Carbon*. 2006, **44,** 1429-1437.
(12) M. W. Smith, I. Dallmeyer, T. J. Johnson, C. S. Brauer, J. S. McEwen, J. F. Espinal and M. Garcia-Perez, *Carbon*. 2016, **100,** 678-692.
(13) S. Prawer, K. W. Nugent, D. N. Jamieson, J. O. Orwa, L. A. Bursill and J. L. Peng, *Chem. Phys. Lett.* 2000, **332,** 93-97.
(14) G. Wen, S. Wu, B. Li, C. Dai and D. S. Su, *Angew. Chem. Int. Ed.* 2015, **54,** 4105-4109.
(15) J. Peng, N. Chen, R. He, Z. Wang, S. Dai and X. Jin, *Angew. Chem. Int. Ed.* 2017, **56,** 1751-1755.
(16) Y. Lou, J. Ma, W. D. Hu, Q. G. Dai, L. Wang, W. C. Zhan, Y. L. Guo, X. M. Cao, Y. Guo, P. Hu and G. Z. Lu, *ACS Catal.* 2016, **6,** 8127-8139.
(17) R. Rahul, R. K. Singh, B. Bera, R. Devivaraprasad and M. Neergat, *Phys. Chem. Chem. Phys.* 2015, **17,** 15146-15155.
(18) A. L. Guimarães, L. C. Dieguez and M. Schmal, *J. Phys. Chem. B.* 2003, **107,** 4311-4319.
(19) Q. Dai, Q. Zhu, Y. Lou and X. Wang, *J. Catal.* 2018, **357**, 29-40.
(20) J. Ma, Y. Lou, Y. Cai, Z. Zhao, L. Wang, W. Zhan, Y. Guo and Y. Guo, *Catal. Sci. Tech.* 2018, **8** (10), 2567-2577.
(21) Y. Zhang, Y. Cai, Y. Guo, H. Wang, L. Wang, Y. Lou, Y. Guo, G. Lu and Y. Wang, *Catal. Sci. Technol.*, 2014, **4**, 3973-3980.
(22) G. Macfie, A. Cooper and M. F. Cardosi, *Electrochimica Acta.* 2011, **56,** 8394-8402.
(23) Z. Zhao, X. Huang, M. Li, G. Wang, C. Lee, E. Zhu, X. Duan and Y. Huang, *J. Am. Chem. Soc.* 2015, **137,** 15672-15675.
(24) R. G. Rao, R. Blume, T. W. Hansen, E. Fuentes, K. Dreyer, S. Moldovan, O. Ersen, D. D. Hibbitts, Y. J. Chabal, R. Schlogl and J. P. Tessonnier, *Nat. Commun.* 2017, **8,** 340.
(25) I. Efremenko, *J. Catal.* 2003, **214,** 53-67.
(26) M. M. Trandafir, L. Pop, N. D. Hădade, M. Florea, F. Neațu, C. M. Teodorescu, B. Duraki, J. A. van Bokhoven, I. Grosu, V. I. Pârvulescu and H. Garcia, *Catal. Sci. Technol.* 2016, **6,** 8344-8354.
(27) T. Ishida, Y. Onuma, K. Kinjo, A. Hamasaki, H. Ohashi, T. Honma, T. Akita, T. Yokoyama, M. Tokunaga and M. Haruta, *Tetrahedron*, 2014, **70,** 6150-6155.
(28) S. Furukawa, Y. Yoshida and T. Komatsu, *ACS Catal.* 2014, **4,** 1441-1450.
(29) L. Huang, P. F. Luo, W. G. Pei, X. Y. Liu, Y. Wang, J. Wang, W. H. Xing and J. Huang, *Adv. Syn. Catal.* 2012, **354,** 2689-2694.
(30) M. J. Beier, J.-M. Andanson and A. Baiker, *ACS Catal.* 2012, **2,** 2587-2595.
(31) L. G. Cançado, K. Takai, T. Enoki, M. Endo, Y. A. Kim, H. Mizusaki, A. Jorio, L. N. Coelho, R. Magalhães-Paniago and M. A. Pimenta, *Appl. Phys. Lett.* 2006, **88** (16), 163106.

(32) J. H. Chen, W. G. Cullen, C. Jang, M. S. Fuhrer and E. D. Williams, *Phys*. *Rev*. *Lett.* 2009, **102** (23), 236805.
(33) J. H. Zhong, J. Zhang, X. Jin, J. Y. Liu, Q. Li, M. H. Li, W. Cai, D. Y. Wu, D. Zhan and B. Ren, *J. Am. Chem. Soc.* 2014, **136** (47), 16609-16617.
(34) L. G. Cancado, A. Jorio, E. H. Ferreira, F. Stavale, C. A. Achete, R. B. Capaz, M. V. Moutinho, A. Lombardo, T. S. Kulmala and A. C. Ferrari, *Nano Lett.* 2011**, 11** (8), 3190-3196.